



**HAL**  
open science

## Upper Pleistocene uplifted shorelines as tracers of (local rather than global) subduction dynamics

H. Henry, V. Regard, Kevin Pedroja, L. Husson, J. Martinod, C. Witt,  
Arnauld Heuret

► **To cite this version:**

H. Henry, V. Regard, Kevin Pedroja, L. Husson, J. Martinod, et al.. Upper Pleistocene uplifted shorelines as tracers of (local rather than global) subduction dynamics. *Journal of Geodynamics*, 2014, 78, pp.8-20. 10.1016/j.jog.2014.04.001 . hal-00968538

**HAL Id: hal-00968538**

**<https://hal.science/hal-00968538v1>**

Submitted on 1 Apr 2014

**HAL** is a multi-disciplinary open access archive for the deposit and dissemination of scientific research documents, whether they are published or not. The documents may come from teaching and research institutions in France or abroad, or from public or private research centers.

L'archive ouverte pluridisciplinaire **HAL**, est destinée au dépôt et à la diffusion de documents scientifiques de niveau recherche, publiés ou non, émanant des établissements d'enseignement et de recherche français ou étrangers, des laboratoires publics ou privés.

1  
2 **UPPER PLEISTOCENE UPLIFTED SHORELINES AS TRACERS OF (LOCAL RATHER THAN**  
3 **GLOBAL) SUBDUCTION DYNAMICS**  
4

5  
6 Hadrien Henry<sup>1,2,3</sup>, Vincent Regard<sup>1,2,3\*</sup>, Kevin Pedoja<sup>4,5,6</sup>, Laurent Husson<sup>7</sup>, Joseph  
7 Martinod<sup>1,2,3</sup>, Cesar Witt<sup>8</sup>, Arnauld Heuret<sup>9</sup>  
8

9 1- Université de Toulouse; UPS GET, 14 avenue E. Belin, F-31400 Toulouse, France

10 2- CNRS; GET ; 14 avenue E. Belin, F-31400, Toulouse, France

11 3- IRD; UR 234, GET ; 14 avenue E. Belin, F-31400, Toulouse, France

12 4- Normandie Univ, France

13 5- UCBN, M2C, F-14000 Caen, France

14 6- CNRS, UMR 6143 M2C, F-14000 Caen, France

15 7- CNRS, ISTERre, Université Joseph Fourier, Grenoble, France

16 8- Université de Lille 1; CNRS ; Géosystèmes, Villeneuve D'Ascq, France

17 9- Département de Géologie; EA4098 LaRGe Labo. de Rech. en Géosciences; Université des  
18 Antilles et de la Guyane, Campus de Fouillol - 97159 Pointe à Pitre Cedex, Guadeloupe,  
19 FWI.

20 \* Corresponding author. E.mail: [Vincent.regard@get.obs-mip.fr](mailto:Vincent.regard@get.obs-mip.fr); Ph : +33 5 61332645  
21

22 **ABSTRACT**  
23

24 Past studies have shown that high coastal uplift rates are restricted to active areas, especially  
25 in a subduction context. The origin of coastal uplift in subduction zones, however, has not yet  
26 been globally investigated. Quaternary shorelines correlated to the last interglacial maximum  
27 (MIS 5e) were defined as a global tectonic benchmark (Pedoja et al. (2011)). In order to  
28 investigate the relationships between the vertical motion and the subduction dynamic  
29 parameters, we cross-linked this coastal uplift database with the "geodynamical" databases  
30 from Heuret (2005), Conrad and Husson (2009) and Müller et al. (2008). Our statistical study  
31 shows that: [1] the most intuitive parameters one can think responsible for coastal uplift (e.g.,  
32 subduction obliquity, trench motion, oceanic crust age, interplate friction and force,  
33 convergence variation, dynamic topography, overriding and subducted plate velocity) are not  
34 related with the uplift (and its magnitude); [2] the only intuitive parameter is the distance to  
35 the trench which shows in specific areas a decrease from the trench up to a distance of ~300  
36 km; [3] the slab dip (especially the deep slab dip), the position along the trench and the  
37 overriding plate tectonic regime are correlated with the coastal uplift, probably reflecting  
38 transient changes in subduction parameters. Finally we conclude that the first order parameter  
39 explaining coastal uplift is small-scale heterogeneities of the subducting plate, as for instance  
40 subducting aseismic ridges. The influence of large-scale geodynamic setting of subduction  
41 zones is secondary.  
42  
43

44 **Highlights**  
45

- 46 - Large-scale geodynamics only explain first order coastal uplift rates  
47 - Uplift is localized over asperities of the subducting plate  
48 - Uplift could be related to transient changes in subduction parameters

49 - Rapid uplift is restricted to the area <300 km from the trench (forearc)

50 - Forearc and plate interiors respond differently

51

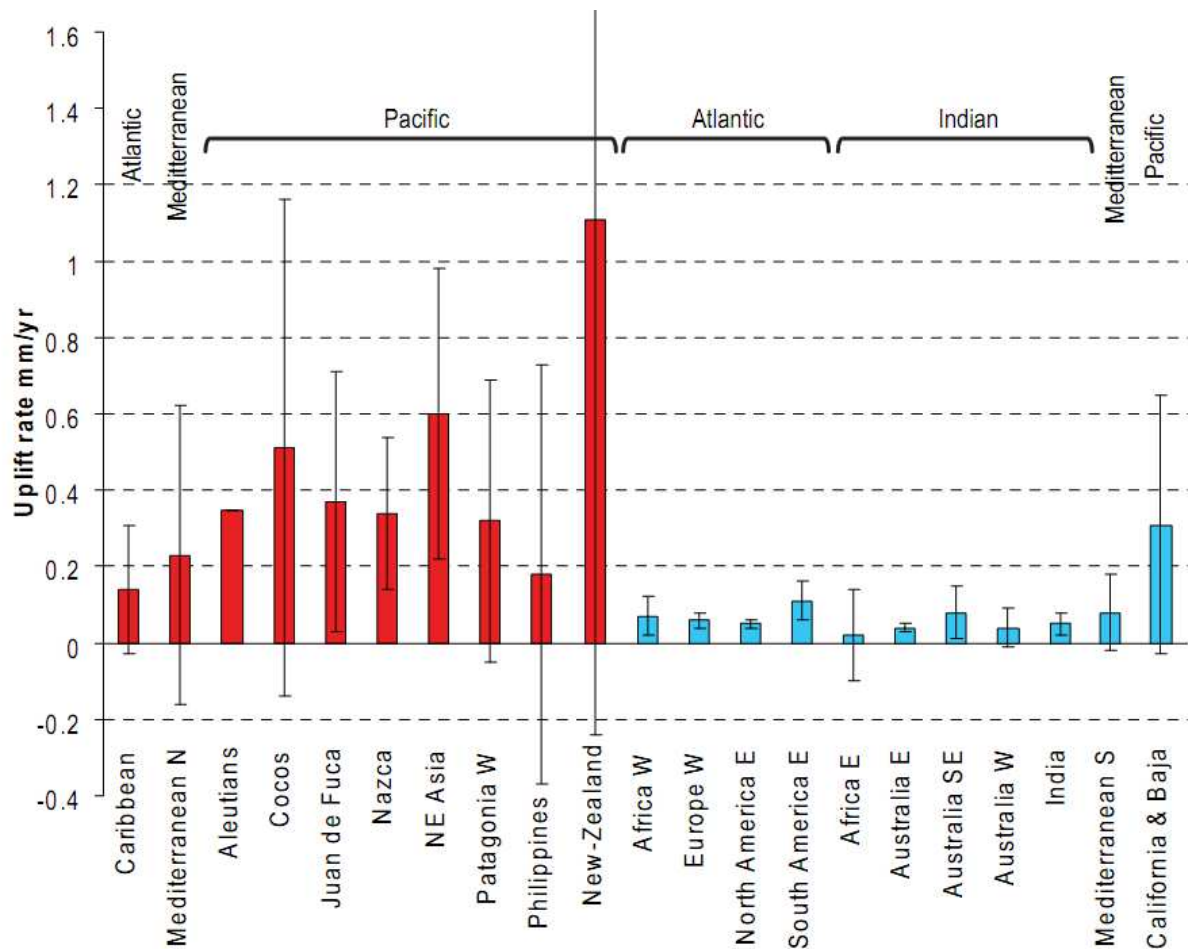
52 **Keywords:** marine strandline; shoreline; uplift; subduction; geodynamics; Quaternary

## 53 1. INTRODUCTION

54

55 Fossil shorelines (or strandlines) are generally packed and constitute staircase coastal  
56 geomorphologies or sequences of "terraces" (e.g. marine or reefal for example). They are  
57 tracers of the sea level at the time they formed. Current elevation of fossil shorelines results  
58 from the combination of sea level change (eustasy) and vertical ground motion (uplift or  
59 subsidence, Lajoie et al. (1991), Pirazzoli et al. (1993)). Pedoja et al. (2011) exhaustively  
60 compiled the worldwide repartition and elevation of the shorelines formed during the last  
61 interglacial sea level highstand (Marine Isotopic Stage 5e, ~120 ka BP) and calculated  
62 apparent coastal uplift rates since that time. More recently, Pedoja et al. (in press),  
63 investigated other benchmarks (MIS 1, 3, 11 and upper shoreline of the sequences) in the  
64 coastal sequences including MIS 5e strandline. Their database highlights the contrast in  
65 tectonic uplift rates between active zones (mainly Pacific Ocean) and passive zones (Atlantic  
66 and Indian Oceans) (Figure1). Even if Pedoja et al. (in press) did a first-order exploration of  
67 uplift record on paleoshorelines in function of the rough geodynamic setting, vertical motion  
68 along the coasts located above subduction zones has never been extensively explored. In this  
69 paper, we look for possible geological parameters that may explain why coastal areas located  
70 above subduction zones are uplifting so fast (Figure 1).

71



72  
73 *Figure 1. Worldwide distribution of apparent coastal uplift rates (since MIS 5e): in red and blue the*  
74 *average uplift rate for, respectively, the actively deforming zones (mostly subduction zones) and the*  
75 *stable zones (mostly passive margins; data from Pedoja et al. (2011). Brackets represent the data*  
76 *standard deviation. Note the zone named California and Baja, corresponds to a passive margin very*  
77 *close to a rift/transform setting.*

78 The compilation from Pedoja et al. (2011) records only emerged terraces with few exceptions.  
79 As discussed in Pedoja et al. (2011), the worldwide distribution of shoreline sequences  
80 suggests that there are much less subsiding areas along subduction coastlines than uplifting  
81 ones, a fact that shall not be considered as an observational bias (see Pedoja et al., 2011,  
82 2014). Then, the database may reflect a global tendency to coastal uplift during late  
83 Pleistocene (Pedoja et al. (2011)), and also partly results from the fact that Pleistocene to  
84 present-day coastal subsidence is more difficult to quantify than coastal uplift. In any case,  
85 this database shows that the average coastal uplift is faster above subduction zones than at  
86 passive margins. In the following, we look for possible links between Late Pleistocene  
87 (posterior to MIS5) coastal uplift and subduction geodynamics. In particular, we investigate  
88 the uplift dependence on some geodynamic parameters, chosen for their driving effect. Some  
89 are obvious, like: distance to the trench, trench motion, age of the subducting plate,  
90 subduction obliquity, overriding and subducting plate velocities, and dynamic topography.  
91 The others are suspected to act on the vertical motion but with magnitudes and direction that  
92 deserve exploration: interplate force and friction force, position along the trench (i.e. distance  
93 to the subducting plate edge), slab dip, tectonic setting of the overriding plate (see Heuret,  
94 2005).

96 **2.1 Databases: paleoshorelines and geodynamics**

97 The compilation by Pedoja et al. (in press); Pedoja et al. (2011) focuses on coastal  
98 geomorphic indicators correlated to the Marine Isotopic Stage 5e (125 ky BP). Indeed,  
99 corresponding terraces are the most extensively preserved and dated. Moreover, MIS 5e is  
100 purportedly the last analogue to the current interglacial and the time span is enough to largely  
101 exceed several seismic cycles such that the uplift rate is not significantly affected by an  
102 individual seismic event. Using the MIS 5e shoreline elevation, we calculated the average  
103 uplift rate using the following formula:  $U=(z-e)/t$ , with  $U$  the shoreline uplift rate,  $z$  the MIS  
104 5e terrace elevation,  $t$  the age of the terrace and  $e$  the relative elevation of the MIS 5e sea level  
105 with respect to the current sea level. In accordance to Pedoja et al. (in press); Pedoja et al.  
106 (2011)), we use  $e= 0\pm 10$  m, which is conservative in the sense it takes into account the  
107 different debated evaluations of the last interglacial sea-level (e.g., Waelbroeck et al. (2002),  
108 Kopp et al. (2009); O'Leary et al. (2013)) and the way the shorelines are fossilized (e.g.,  
109 Lajoie et al. (1991)). In addition, this elevation value is of little interest to the current study as  
110 it uniformly offsets uplift rates while our analysis considers relative vertical displacements  
111 from one site to another. Besides the elevation of the uplifted shorelines, Pedoja et al. (in  
112 press; 2011) deliver some additional information like the geographic location of the  
113 sequences. Noteworthy, the spatial repartition of the data over South America, Japan and  
114 Cascadia subduction allow investigating the coastal uplift distribution as a function of the  
115 distance to the trench up to 800 km away (in the Japan and South America transects). In  
116 addition, it is noticeable that some places have not been investigated for marine terraces, like  
117 the Aleutian subduction zone where the Ostrov Beringa and Seguam islands exhibit marine  
118 terraces visible on satellite images but not studied in the field or even the Mariana subduction  
119 zone (Stafford et al. (2005) observed uplifted karst in Guam).

120  
121 Subduction zone geodynamic parameters are sourced from Heuret (2005)(parts of the data  
122 base have been published in Heuret & Lallemand, 2005, Lallemand et al., 2005 and Funiciello  
123 et al. 2008). He provides every 2 degrees multiple geodynamic parameters like the overriding  
124 plates tectonic regime, the trench motion, the proximity of the measurement to a subduction  
125 edge, the shallow and deep slab dip, the age of the adjacent oceanic crust and the plate  
126 convergence rate. In addition, we extracted the current dynamic topography rate of change for  
127 the last Myr from the dynamic topography data released by Conrad and Husson (2009) and  
128 Müller et al. (2008). Besides end-member models HS3 (Gripp and Gordon 2002) or NNR ,  
129 most of the reference frames fall in the same range (see e.g. fig.6 in Becker, 2006). Given  
130 that, we chose the moving hotspot model of Steinberger et al. (2004) to calculate the trench,  
131 the overriding and subducting absolute plate motion because we see it as representative of  
132 most frameworks (see Funiciello et al for some comparisons between frameworks). Thus, we  
133 emphasize that our observations and conclusions would not be altered by choosing an  
134 alternative reference frame. The reference frame defined by Steinberger et al. (2004) is very  
135 similar to that of O'Neill et al. (2005) which is based on the Indo-Atlantic hotspots. Such  
136 reference frames are most in line with predictions from geodynamic models where subducting  
137 plates move trenchward and trenches predominantly retreat and where global mantle viscous  
138 dissipation is minimized, while this is not the case for HS3 (Schellart et al., 2008). Second,  
139 Indo-Atlantic hotspots reference frames are in better agreement with observed global mantle  
140 anisotropy than HS3 (Becker et al., 2008, Kreemer, 2009) and with subducted slab structure  
141 than HS3 (Schellart, GRL 2011). The convergence rates are extracted from Heuret (2005)  
142 (published in Lallemand et al., 2005).

143 The interplate friction force is calculated after Lallemand (1999) assuming a friction  
144 coefficient of 0.3. The interplate force at trench is probably best expressed as the mean trench  
145 normal integrated mantle drag called  $M_d$  and calculated by Husson (2012). This metric  
146 averages the drag forces exerted by the convecting mantle underneath the converging plates.  
147 This value is the integral of the normal to trench components of the shear tractions derived  
148 from Conrad and Behn (2010) or Conrad and Husson (2009). As, such  
149 it is a measure of the net horizontal force that drags plates against each other. Husson (2012)  
150 proposed this value to be best correlated to the upper plate tectonic setting (see thereafter,  
151 section 3.3).

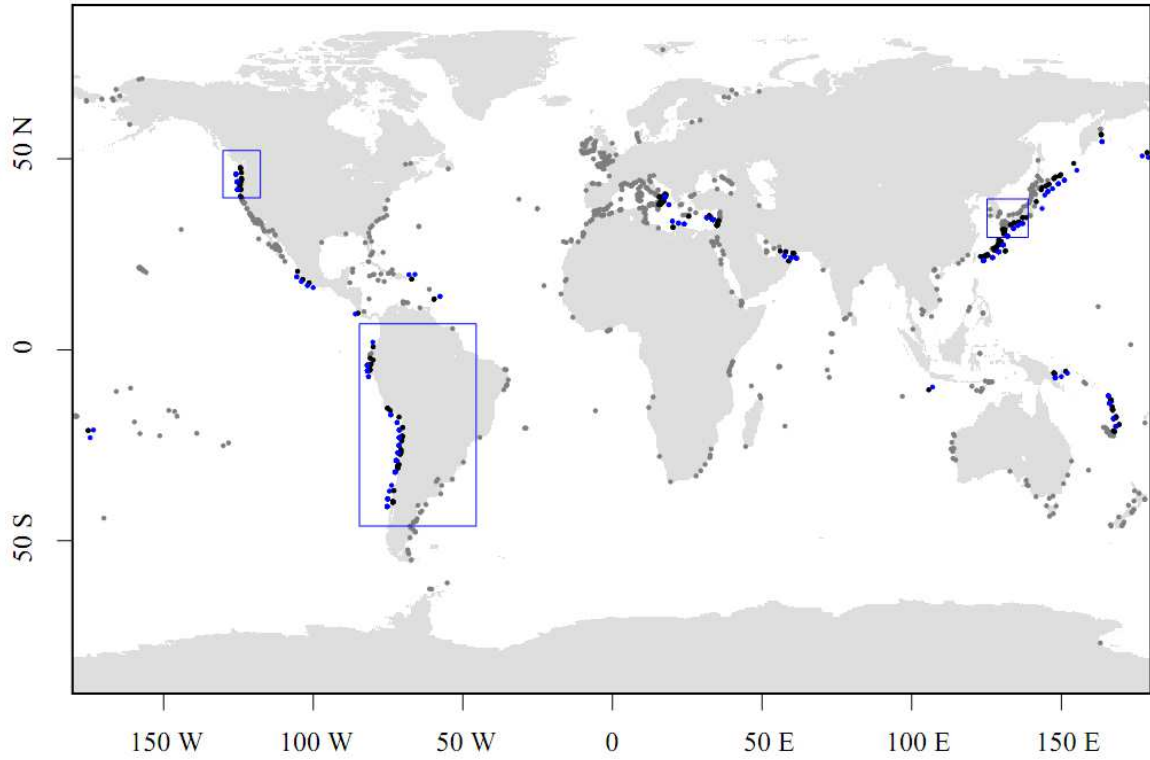
152 The Mediterranean Sea has been avoided by Heuret (2005) because subduction zones are  
153 small and possibly interact with each other and surrounding collision zones. The dataset of  
154 Heuret (2005) is here extended to encompass the Mediterranean Sea (Gibraltar, Tyrrhenian  
155 and Aegean subduction zones) and the Makran (Figure 2A).

156  
157 Finally, we combine the 2 datasets (uplifted shorelines from the last interglacial maximum vs.  
158 subduction geodynamics), by associating each site of uplifted shoreline to the closest  
159 subduction data point in 2 degree-bins. Figure 2 shows the spatial repartition of the uplifted  
160 paleocoasts (shoreline, strandline, etc.) and related subduction record. The average uplift rate  
161 derived from the marine terraces in this record is  $\sim 0.2227$  mm/y.

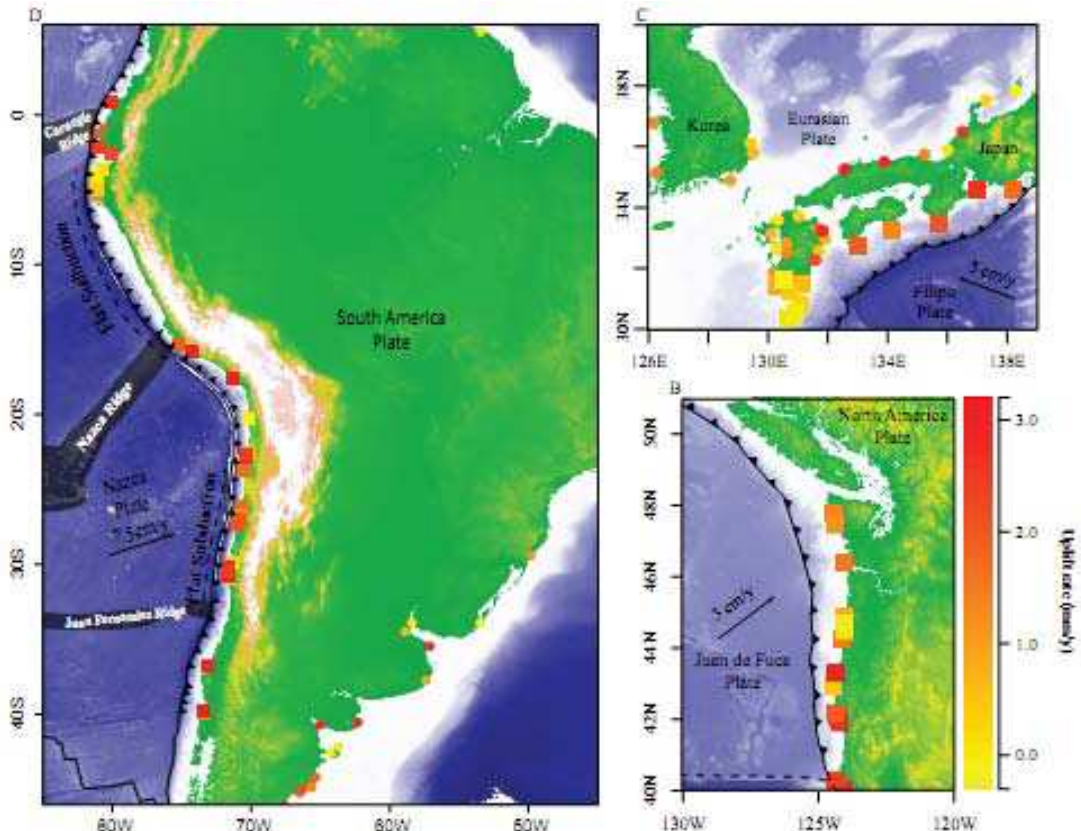
162  
163 In order to define a robust indicator of correlation between the apparent coastal uplift rate and  
164 the various geodynamic parameters that we tested, we calculated correlation coefficients  $r$  as  
165 defined by Pearson (1896):

166 
$$r = \frac{\sum_{i=1}^n (x_i - \bar{x})(y_i - \bar{y})}{\sqrt{\sum_{i=1}^n (x_i - \bar{x})^2 \sum_{i=1}^n (y_i - \bar{y})^2}}$$

167 where  $x_i$  and  $y_i$  are data coordinates and  $\bar{x}$  and  $\bar{y}$  their average values. A correlation coefficient  
168 of 1 or -1 would respectively indicate a perfect linear correlation or anti-correlation between  
169 the uplift rate and the tested parameter. Every data manipulation and calculation has been  
170 performed with the software RGui (R Development Core Team (2010)). Note that this  
171 correlation coefficient is ineffective to account for non-linear relationships. We will qualify of  
172 'significant' every correlation coefficient associated with a p-value < 0.01. This always comes  
173 with a  $1\sigma$  confidence interval encompassing the 0 value.



175 A



176  
177  
178  
179  
180  
181

*Figure 2. A. Spatial repartition of the two main databases: the MIS 5e uplifted shoreline data from Pedoja et al. (2011) are in grey or black if less than 2 degrees away from any subduction data (Heuret and Lallemand, 2005); the subduction data, in blue is only pictured if MIS5e uplifted shoreline data are associated. The blue boxes display the three places where records are suitable to observe the uplift rate distribution along a trench perpendicular transect. B to D, zoom on areas of*

182 *special interest (see transects, sections 2.2 and 3.1); colours represent the uplift rate and the symbol*  
183 *(square/circle) represent the location of data less/more than 2degrees away from the trench.*

## 184 **2.2 Geological context of the South America, Cascadia and Japan-Korea** 185 **margins**

186 We found 3 places in the world where a repartition of terrace data from the fore-arc area  
187 toward the inner upper plate is available (Figure 2): the Juan de Fuca plate subduction under  
188 the Cascades, the Nazca plate subduction under South America and the Philippine Sea plate  
189 subduction under Japan and Korea. The Juan de Fuca plate subduction zone extends  
190 ~1000 km from the north of the Mendocino triple point to the south of the Queen Charlotte  
191 Island (51°N/130°W; 40°N/110°W). The subduction obliquity varies from 30° to the south to  
192 15° to the north with a plate convergence rate estimated at 3.1 cm/y (Heuret and Lallemand,  
193 2005). The age of the oceanic crust entering the trench is 10 My (Müller et al. (1997)). The  
194 tectonic setting of the overriding plate varies from slightly extensive to the south to mostly  
195 wrench faulting to the north (E1 to 0 as described thereafter; Heuret and Lallemand, 2005).  
196 The distance between the location of uplift data and the trench varies between 60 and 135 km  
197 (Figure 3B). The upper plate lithosphere elastic thickness is 10-30 km (Lowry et al. (2000)).

198 Coastal sequences on the Japan/Korea coasts are located above the Nankai-Ryukyu  
199 subduction zone where the Philippine Sea plate subducts below the Eurasian plate. This area  
200 extends latitudinally from Tokyo to Pyongyang, and from Honshu Island to the Tanega-Shima  
201 Island from E to W (40°N/126°E; 30°N/139°E). The obliquity of the subduction ranges from  
202 20° to the west to 40° to the east (Heuret and Lallemand, 2005). Plate convergence in this area  
203 is 4.8 cm/y and the oceanic crust entering the trench is 35 My-old (Müller et al. (1997)). The  
204 tectonic setting of the Eurasian plate is slightly compressive on the whole studied segment  
205 (C1 as described thereafter) (Heuret and Lallemand, 2005). In this area, the distance between  
206 uplift data and the trench varies between 60 and 900 km (Figure 3A).

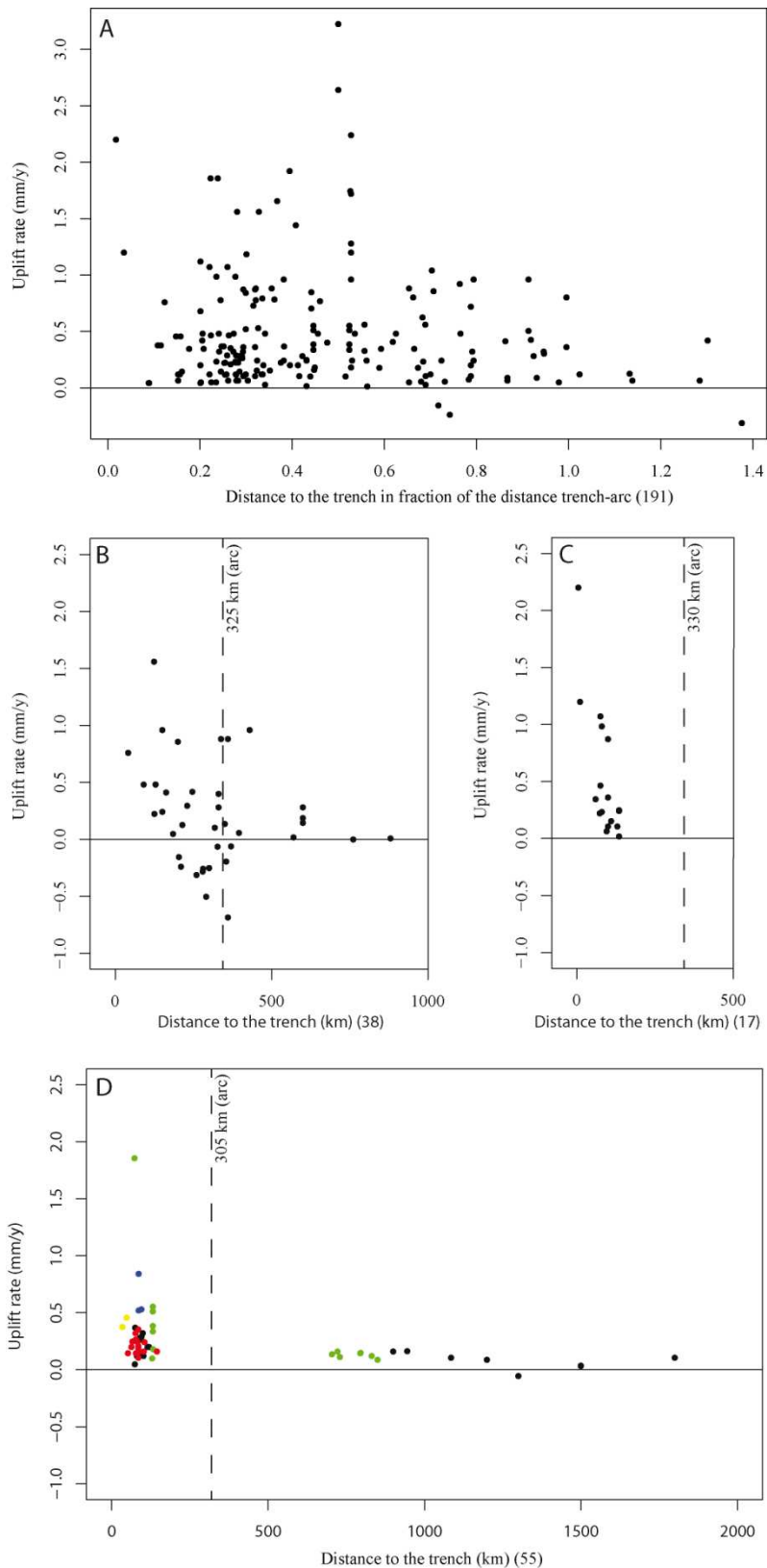
207 The South American area analyzed in this study is located along the ~6000 km-long Nazca  
208 subduction zone (from 5°N to 45°S, figure 2D). The Nazca subduction presents several  
209 particular zones of interest: the Carnegie ridge (0.5°N to 2°S; Gutscher et al. (1999a)), the  
210 Peruvian flat subduction (2 to 15°S, Gutscher et al. (1999b)), the Nazca ridge entrance into  
211 subduction (13 to 16°S; e.g., Machare and Ortlieb (1992), Hampel (2002), Espurt et al.  
212 (2008), Saillard et al. (2011)) and the Andean flat slab region which is located between 27 and  
213 32° S (Yañez et al. (2001)). Plate convergence in this area is about 7 cm/y and the oceanic  
214 crust entering into the trench is 0 to 40 My-old (Müller et al. (1997); Heuret and Lallemand,  
215 2005). Subduction obliquity is everywhere smaller than 20°. The South American plate  
216 tectonic setting presents a North to South compression gradient (Heuret and Lallemand,  
217 2005), from compressive in Central Andes to neutral in Southern Andes; its elastic thickness  
218 possibly strongly varies from less than 10 km along the arc to >50 km in the foreland (Tassara  
219 (2005); Tassara et al. (2007)).

## 220 **3. RESULTS**

### 221 **3.1 Distance to the trench**

222



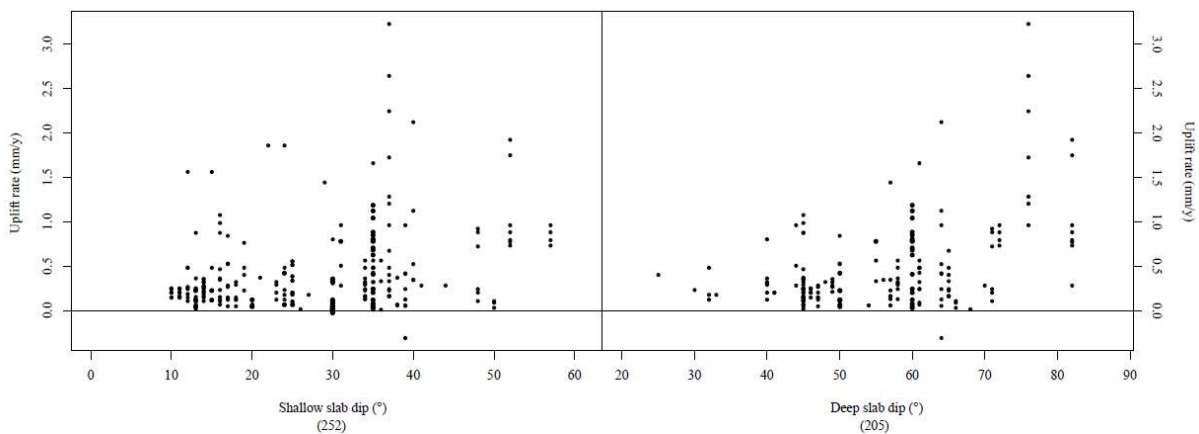


223  
 224  
 225  
 226  
 227  
 228

*Figure 3. Uplift rate versus distance to the trench. A: All data, expressed in function of the trench-arc distance. B: Philippine Sea plate subduction. C: Cascadia subduction. D: Nazca subduction; data located above the Peruvian and the Juan Fernandez flat subduction areas are shown in red (2-15°S and 27-32°S), over the Nazca Ridge in blue (13-16°S) and over the Carnegie Ridge in yellow (0.5°N-2°S). In addition green points are data from Patagonia (south of 32°S).*

229 The distance to the trench anti-correlates with uplift rates (Figure 3). Higher uplift rates are  
 230 found at the closest points to the trench in every transect (Figure 3). Uplift rates generally  
 231 decrease with the distance to the trench, with sometimes an area of slower uplift (e.g.,  
 232 negative values at ~300 km from the trench in Japan, Figure 3B). A direct correlation between  
 233 the distance to the trench and the uplift rate is clear close to the trench, less clear farther. The  
 234 overall relation is marked by a negative correlation coefficient of -0.12 (<-0.24 for each  
 235 individual zone, table 3), quite significant (p-value of 0.03), which is meaningless considering  
 236 the trend is non-linear (it becomes non-linear when considering points farther than the arc,  
 237 Figure 3). We observe that the area of strong uplift is restricted to the first ~300 km from the  
 238 trench, corresponding to the forearc area.

### 239 3.2 Slab dip

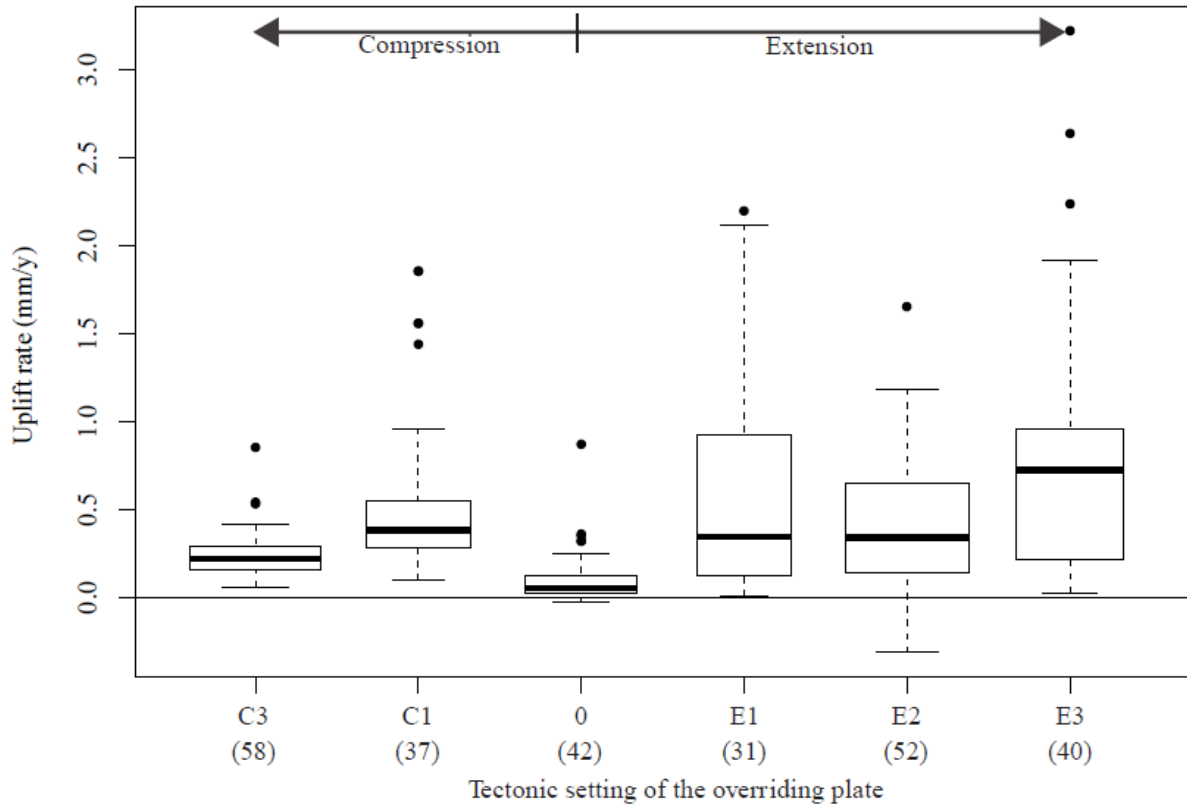


240 *Figure 4. Left: uplift rate vs. shallow slab dip; right: uplift rate vs. deep slab dip, for the entire*  
 241 *dataset.*

242 Slab dip is measured at shallow depth (average dip between 0 and 125 km depth); and at  
 243 greater depth, (average dip between 125 and 670 km depth)(Heuret and Lallemand, 2005).  
 244 For both shallow and deep slab dip datasets, corresponding uplift rate appears to increase with  
 245 slab dip (Figure 4). For the shallow slab dip the correlation is not obvious but marked by a  
 246 slightly positive correlation coefficient of 0.32. The deep slab dip does not seem to influence  
 247 the uplift rate below a critical value of ~60 degrees; above this value, there is a positive  
 248 correlation between deep slab dip and surface uplift (Figure 4).

### 249 3.3 Tectonic setting of the overriding plate

250 Figure 5 shows the variations of uplift rate in function of the tectonic regime of the overriding  
 251 plate. Heuret (2005) and Heuret and Lallemand (2005) describe the tectonic regime of the  
 252 overriding plate using recorded focal mechanisms and classify it from the very compressive  
 253 (C3) to very extensive (E3), 0 being neutral (no focal mechanism or wrench faulting). For this  
 254 kind of qualitative parameter, it is not possible to calculate a correlation coefficient. We rather  
 255 study them qualitatively, using boxplots (sometimes called box-and-whisker plots Tukey,  
 256 1977).  
 257



258  
 259 *Figure 5. Uplift rate as a function of the overriding plate tectonic setting as defined by Heuret and*  
 260 *Lallemand (2005). C3 is considered to be the most compressive state while E3 is the most*  
 261 *extensional. C2 is absent because no C2 area is related to MIS5e marine terraces. Data number*  
 262 *appears in parentheses under each box. Additional information can be found in Table 1. Horizontal*  
 263 *bars indicate, from the bottom to the top, the first decile, the first quartile, the median, the third*  
 264 *quartile and the ninth decile; dots are outliers. The horizontal size of the box is function of the data*  
 265 *number.*

266 Figure 5 shows a slight tendency to greater uplift rates when the tectonic setting is extensional  
 267 rather than compressive. Noteworthy, intermediate settings (C1 to E2) are quite similar while  
 268 the main trend comes from the extremes (C3 and E3 tectonic settings).  
 269

270 *Table 1. Mean uplift rates (mm/yr) as a function of the tectonic setting of the overriding plate (C3*  
 271 *to E3) and for the position along the subduction zone expressed in “far” or “at” slab edge.*

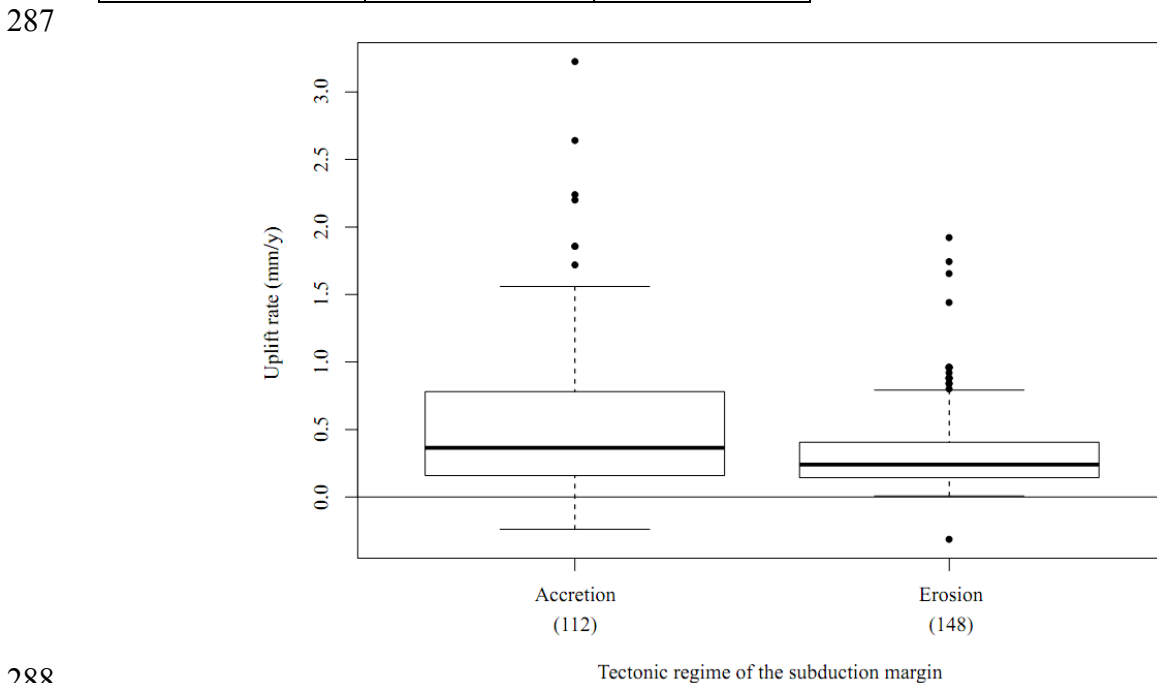
	C3	C2	C1	0	E1	E2	E3	At slab edge	Far from slab edge	Accretionary margins	Erosive margins
1 <sup>st</sup> quartile	0.144	NA	0.280	0.020	0.120	0.144	0.212	0.100	0.144	0.160	0.144
Median	0.208	NA	0.384	0.054	0.344	0.340	0.724	0.328	0.240	0.364	0.244
3 <sup>rd</sup> quartile	0.280	NA	0.550	0.120	0.928	0.652	0.950	0.872	0.364	0.780	0.406
Number of	58	NA	37	42	31	52	40	113	147	112	148

data											
------	--	--	--	--	--	--	--	--	--	--	--

272  
 273 Figure 6 shows the relation between the uplift rate and the tectonic regime of the subduction  
 274 margin. Accretionary margins show a higher magnitude (median: 0.36 mm/yr instead of 0.24  
 275 mm/yr for erosive ones) and a greater variability in uplift rate than erosive margins. The  
 276 difference between those two regimes is somewhat significant: the median value for the  
 277 accretionary margin (0.36 mm/y) corresponding to the third quartile value of the erosive  
 278 margins (0.41 mm/y). The frequency of observation of uplift/subsidence in accretionary and  
 279 erosive margins does not differ significantly (Table 2). This, together with the figure 6 pleads  
 280 for a more variable vertical motion at accretionary margins than at erosive ones but without  
 281 preferential (uplift/subsidence) direction.

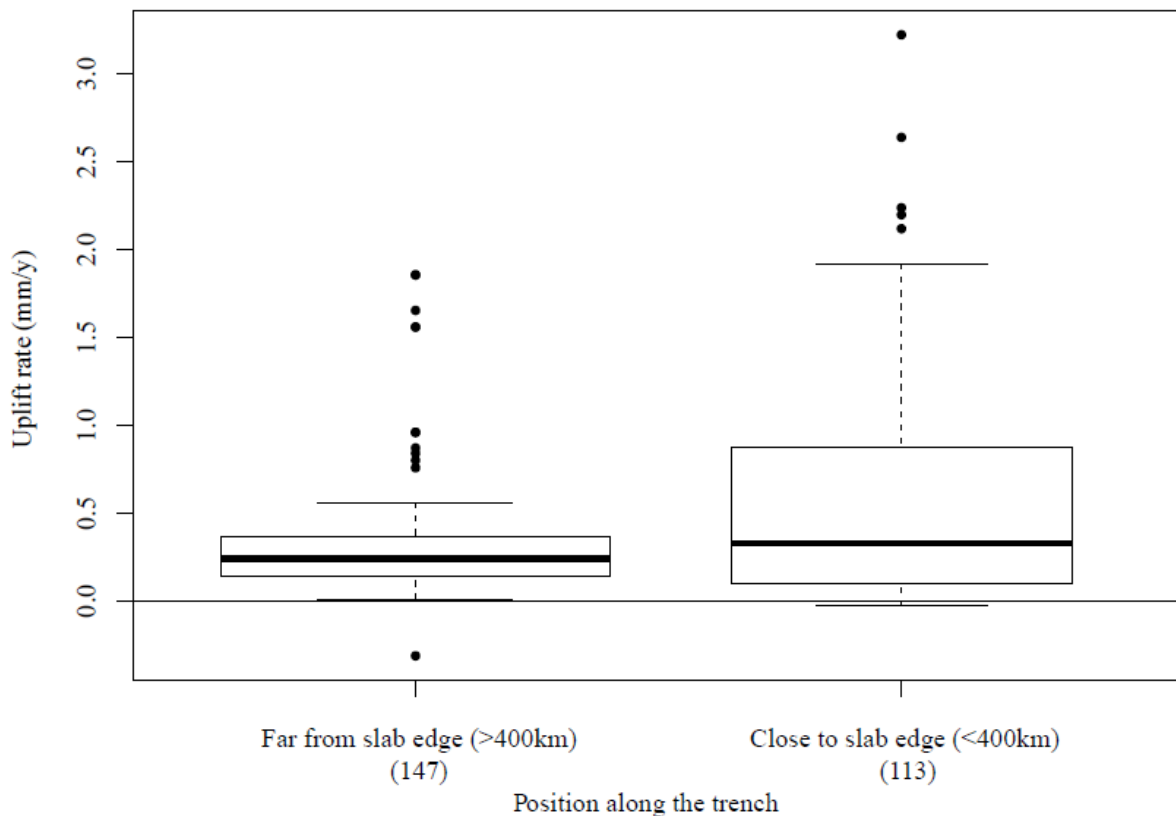
282  
 283 *Table 2. Number of data showing uplift, subsidence as function of the subduction margin tectonic*  
 284 *setting. It reads as following example: the dataset of accretionary margins over 139 data, 26 (19%)*  
 285 *record uplift and 2 (1%) record subsidence. There is no vertical motion data for the remaining 111*  
 286 *(80%) data.*

	Accretionary	%	Erosive	%
Number of data	139		121	
Uplift	26	19	40	33
Subsidence	2	1	1	1
No associated data	111	80	80	66



288  
 289 *Figure 6. Uplift rate as a function of the subduction margin tectonic setting. See caption of Figure*  
 290 *5 for description of figure. Data number appears in parentheses under each box.*

291



293 *Figure 7. Uplift rate versus distance to a subduction edge. See caption of Figure 5 for description of*  
 294 *figure. Data number appears in parentheses under each box. Additional information can be found*  
 295 *in Table 1.*  
 296

297 The position along the trench may be an important parameter as emphasized by the particular  
 298 tectonic setting of slab lateral boundaries (Funiciello et al. (2004); Lallemand et al. (2005);  
 299 Schellart et al. (2011)). According to Lallemand et al. (2005), a datum is considered to be at a  
 300 subduction edge if it is closer than four degrees from the edge of the subduction. The uplift  
 301 rate is shown as a function of the proximity of the measurement to a slab edge in figure 7.  
 302 This figure shows that slab edges are characterized by higher uplift rates than elsewhere along  
 303 the subduction zone. The difference is somewhat significant: the median value at slab edge  
 304 corresponds to the third quartile value far from the edges (average uplift rate of 0.33 and 0.36  
 305 mm/y, respectively, Table 1).

### 306 **3.5 Dynamic topography**

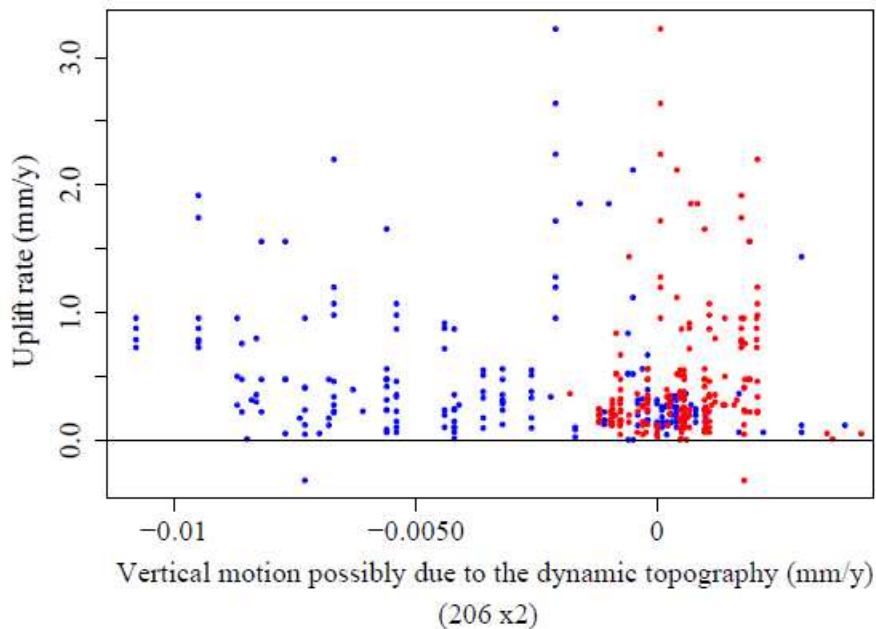
307 Temporal changes in dynamic topography can offset sea level relative to the continent. A local  
 308 decrease in dynamic topography leads to sea transgression while and conversely, an increase  
 309 will produce continent emersion, regression, marine terrace fossilization and uplift. Thus we  
 310 calculated the rate of change in dynamic topography through the last million years. Two  
 311 models of dynamic topography change have been tested (Conrad and Husson (2009); Müller  
 312 et al. (2008)). Combination of the 2 datasets (coastal uplift and dynamic topography) was  
 313 performed in a 0.5 degree-bin because of the high apparent resolution of the dynamic  
 314 topography models. Table 3 shows the comparison between the average observed uplift and  
 315 the average vertical ground motion possibly due to changes in the dynamic support of the  
 316 topography. Figure 8 shows the relationship between the rate of change in the modelled  
 317 dynamic topography and measured uplift.

318  
 319  
 320  
 321  
 322  
 323

*Table 3. Comparison of the observed uplift (Pedoja et al. (2011)) with modelled dynamic topography rates of change at the same locations (Conrad and Husson (2009); Müller et al. (2008)). The values are the average of 0.5 degrees bins regarding subduction zones. Note that the uplift observed from Pedoja et al. (2011) consequently differs from the average values of the entire set of observations (0.2227 mm/yr).*

	Average uplift rate since the MIS 5e (mm/y)	Average uplift since the MIS 5e (m)
Observed uplift from Pedoja et al. (2011)	0.3533	44.16
Dynamic topography after Conrad and Husson (2009)	0.005	0.625
Dynamic topography after Müller et al. (2008)	-0.029	-3.625

324



325  
 326  
 327

*Figure 8. Uplift rate versus rate of change in dynamic topography for the last Ma.; in red, after Conrad and Husson (2009); in blue, after Müller et al. (2008).*

328 According to the tested dynamic topography models, the average contribution to the vertical  
 329 motion would be one order of magnitude underneath the observed uplift. In addition to this,  
 330 figure 8 and the related correlation coefficient prevent from stating that there is a significant  
 331 link between the dynamic topography and the observed coastal uplift rate. Last, the fact that  
 332 most coastlines are uplifting suggests that dynamic topography shall not explain this  
 333 phenomenon; indeed, uplift and subsidence must overall cancel each other and average to  
 334 zero.

### 335 3.6 Other parameters

336 The other tested parameters do not show any trend with coastal uplift. Their correlation  
 337 coefficient is too low to conclude on the robustness of any link between the measured uplift  
 338 and tested geodynamic parameters. Among these, we explored the correlation of uplift rates  
 339 with the commonly invoked overriding and subducting plate velocities, trench motion,  
 340 convergence acceleration, subduction obliquity, oceanic crust age, interplate force and friction

341 force. Figure 9 summarizes the relationship between all the aforementioned parameters and  
342 the coastal uplift.

### 343 **Plate and trench motion**

344 The absolute plate motion comes from Steinberger et al. (2004). In Figure 9 A and B, positive  
345 (negative) values of subducting or overriding absolute plate motion indicate a movement  
346 toward (away from) the trench. The normal overriding plate velocity does not appear to be  
347 correlated with the uplift rate. Although the normal subducting plate velocity visually seems  
348 slightly correlated to the uplift rate the correlation coefficient is nearly null ( $\sim 0.02$ ) (Figure  
349 9B). Finally, the convergence velocity is also surprisingly not correlated with terrace uplift  
350 (Figure 9A), even if we only take into account the trench-normal convergence velocity  
351 (Figure 9B). No correlation between trench motion and uplift rate is detectable (Figure 9C).  
352 In addition we evaluated the current change in convergence velocity for the plates involved in  
353 the Tonga-Kermadec, Japan, South America, Aleutian and Cascadia subduction (Figure 9D)  
354 by comparing a compilation of GPS derived, instantaneous velocity data (Sella et al. (2002))  
355 to the integrated velocity for the last 3.2 Ma (NUVEL-1A, De Mets et al. (1994)). It is not  
356 possible to derive any correlation since the plate velocity change is distributed in patches.  
357 Anyway, the visual inspection does not plead for any correlation.

### 358 **Obliquity**

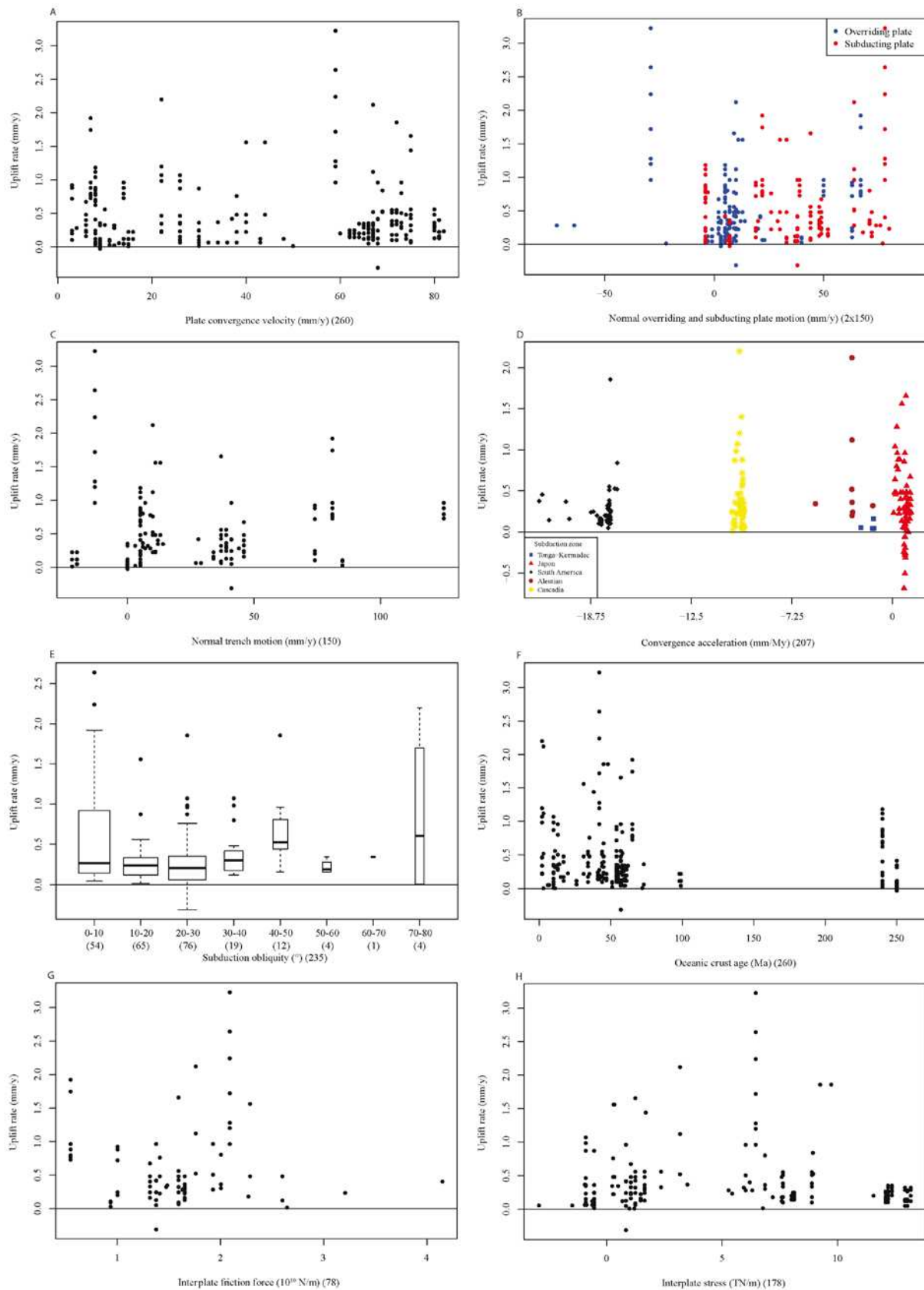
359 The subduction obliquity is calculated using DeMets et al. (1994) NUVEL-1A plate velocity  
360 model and Heuret (2005)'s trench azimuth (Figure 9E). An obliquity value of  $0^\circ$  indicates a  
361 perfectly orthogonal subduction. The dataset covers a wide range of obliquity values that are  
362 well distributed. No trend is observed except a possible slight increase towards normal  
363 convergence.

### 364 **Oceanic crust age**

365 The oceanic crust age is compiled by Heuret and Lallemand (2005) after Müller et al. (1997)  
366 and indicates the age of the oceanic crust at the trench. This distribution is not correlated with  
367 the uplift rate.

### 368 **Interplate friction force and interplate force**

369 Figure 9G shows the interplate friction force (*sensu* Lallemand, 1999) vs uplift rate. The  
370 interplate force is estimated by Husson (2012) by calculating the mean of the integrated  
371 mantle drag from both the overriding and subducting plate ( $M_d$ ). There is detectable uplift rate  
372 correlation neither with the interplate friction force nor with  $M_d$  (Figure 9G & H).



373

374 *Figure 9. A: Uplift rate as a function of the convergence rate; B: Uplift rate as a function of the*  
 375 *overriding (blue) and subducting plate (red) absolute motion; C: Uplift rate as a function of the*  
 376 *absolute trench motion; D: Uplift rate as a function of the convergence variation for the last 3.2*  
 377 *Myrs, as the difference between NUVEL-1A and REVEL models, the different subduction zones are*



378 *pictured; E: Uplift rate as a function of the convergence obliquity; F: Uplift rate as a function of*  
 379 *the oceanic crust age at the trench; G: Uplift rate as a function of the interplate friction force. H:*  
 380 *Uplift rate as a function of the interplate force.*

#### 381 4. SUMMARY AND DISCUSSION

382

383 *Table 4. Linear correlation coefficient between the tested geodynamic parameters and the coastal*  
 384 *uplift. Bold lines indicate significant correlation (or anticorrelation) (p-values < 0.01).*

Geodynamic Parameter	Correlation coefficient	Confidence interval (1 $\sigma$ )	p-values
Subduction obliquity	0.019	[-0.04 0.082]	0.757
Oceanic crust age	-0.148	[-0.208 -0.087]	0.016
Normal Trench motion	0.072	[-0.0101 0.153]	0.382
Interplate force	-0.06	[-0.134 0.015]	0.427
Interplate friction force	0.03	[-0.085 0.144]	0.795
Overriding plate velocity	0.026	[-0.056 0.108]	0.748
<b>Subducting plate velocity</b>	<b>0.239</b>	<b>[0.160 0.315]</b>	<b>0.003</b>
<b>Shallow slab dip</b>	<b>0.286</b>	<b>[0.219 0.350]</b>	<b>4.80x10<sup>-5</sup></b>
<b>Deep slab dip</b>	<b>0.431</b>	<b>[0.368 0.490]</b>	<b>1.70x10<sup>-9</sup></b>
Convergence velocity	0.015	[-0.047 0.077]	0.805
Normal convergence velocity	0.203	[0.124 0.280]	0.012
Convergence acceleration since 3.2 Ma	0.051	[-0.018 0.120]	0.467
<b>Distance to the trench (boxes)</b>	<b>-0.28</b>	<b>[-0.366 -0.189]</b>	<b>0.003</b>
Distance to the trench, in fraction of the distance trench-arc	-0.119	[-0.189 -0.047]	0.031
<b>Distance to the trench (South America transect)</b>	<b>-0.355</b>	<b>[-0.469 -0.229]</b>	<b>0.007</b>
Distance to the trench (Japan-Korea transect)	-0.248	[-0.400 -0.088]	0.128
<b>Distance to the trench (Cascadia transect)</b>	<b>-0.769</b>	<b>[-0.858 -0.637]</b>	<b>3.00x10<sup>-4</sup></b>
<b>Dynamic topography (Conrad and Husson (2009))</b>	<b>0.191</b>	<b>[0.123 0.257]</b>	<b>0.005</b>
<b>Dynamic topography (Müller et al. (2008))</b>	<b>-0.229</b>	<b>[-0.294 -0.162]</b>	<b>9.10x10<sup>-4</sup></b>
Overriding plate tectonic setting	Gently correlated		
<b>Position along the trench</b>	<b>Significantly correlated</b>		
Tectonic regime of the subduction margin	Gently correlated		

385

386 Table 4 summarises the correlation between observed uplift rates and all tested parameters.  
 387 Overall, most of the investigated geodynamic parameters do not seem to influence the uplift  
 388 rate. We additionally observed higher uplift rates near lateral slab boundaries. Lallemand et al.  
 389 (2005) observe that slab dip is generally higher at slab edge. Slab edges are also known to be  
 390 places of high upper mantle toroidal motion, and eventually mantle vertical flow (e.g.,  
 391 Funicello et al. (2006); Guillaume et al. (2010); Schellart et al. (2007)). This leads to  
 392 important variations in geodynamics at slab edges (Schellart et al. (2011)). Out of all the  
 393 tested parameters, two parameters are highly correlated to uplift. First, slab dip shows some  
 394 correlation with the uplift rate. Lallemand et al. (2005), in turn, show that the slab dip

395 correlates to the overriding plate tectonic setting. The higher the slab dip is, the more  
396 extensive the regime of the overriding plate will be. It is fully coherent with the fact the  
397 tectonic setting appears to be linked with uplift rate. But its effect is quite counterintuitive  
398 since uplift is possibly related to extension and low uplift to compression.

399 Due to the quasi-absence of subsiding data, it is not possible to tell if accretionary margins are  
400 more prone to uplift (and less prone to subsidence) than erosive ones, as shown by the works  
401 on subduction tectonic erosion (e.g., Lallemand et al., 1992). However, noticeable is the fact  
402 that erosive margins are not devoid of uplift zones despite the fact that intuitively, the forearc  
403 material loss associated with tectonic erosion is likely to promote subsidence. The normal  
404 faults that have been described in most erosive margins (e.g., Clift and Vannuchi, 2004)  
405 should be responsible of the observed uplifts. The difference between erosive/accretionary  
406 margins is best expressed in terms of variability of the uplift magnitude, greater for  
407 accretionary margins. Large uplifts at erosive margins are possibly inhibited by the forearc  
408 material related to the erosive processes.

409 Second and maybe the best correlated parameter to uplift is the distance to the trench which  
410 shows in 3 particular transects a rapidly slowing uplift with the distance: we evaluated the  
411 characteristic distance of action of the trench to be  $\sim 300$  km, i.e., the trench-arc distance.

412 The main limitation of our approach is the small number of sites evidencing coastal  
413 subsidence, partly because measuring subsidence is more difficult than measuring uplift,  
414 partly because it is less common. For example, this excludes the Sunda subduction zone due  
415 to a lack of observational data. Even if we consider the record is correct for uplifting areas,  
416 the input of subsiding areas could enlarge the range of parameters to observe. For example,  
417 extrapolating the regression observed for steeply dipping slabs toward gentle dips predict  
418 negative values, i.e., subsidence. This will have to be investigated.

419 Another limitation is that “simple” subduction zones associated with a coastline prone to  
420 record fossil shores are not so frequent. For example the Tonga-Kermadec and Marianas  
421 subduction zones are ocean-ocean subduction zones, with limited subaerial exposure in which  
422 vertical displacements can be measured.

423

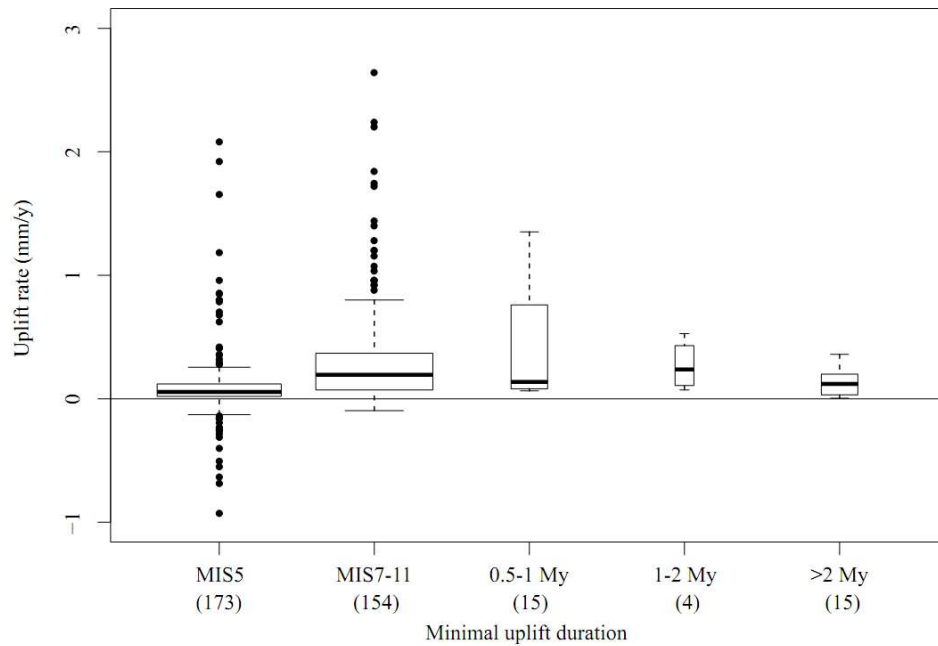
424 A possible reason for the poor correlation between uplift and the geodynamic parameters of  
425 subduction zones is that subduction zones correspond to a long-term phenomenon that lasts  
426 tens of Myrs. In contrast, the analysis of terraces associated with the MIS5e isotopic stage  
427 evidences short term ( $\sim 10^5$  years) vertical displacements. Subductions zones evolve slowly  
428 through time and their morphology should be in equilibrium with the main geodynamic  
429 parameters such as the convergence velocity or the friction at the plate interface. One can  
430 expect that short-term coastal uplift (or subsidence) is mostly due to changes in these  
431 parameters. We thus explored the variation in subduction velocity and the variation in the  
432 dynamic topography but here again we fail at finding any correlation. Finally, the absence of  
433 correlation between geodynamics and vertical motion may plead for a local effect (or short in  
434 time) causing strong vertical motion. These local effects are preferentially due to roughness of  
435 the subducting plate as we illustrate by the examples in the following.

436 (1) In fact, the high uplift rate of E3 (strongly extensive) tectonic setting can come from the  
437 position of E3 data close to slab edges (38 data over 40). The north New Hebrides (Vanuatu)  
438 subduction zone is typical from E3 tectonic setting. It is marked by back-arc opening but also  
439 by many plateau/ridges entering into subduction (Taylor et al. (2005)), probably causing a  
440 high variability in uplift rates. They range 0.004-1.896 mm/y, with a median uplift rate of  
441  $\sim 0.756$  mm/y, close to the median value for E3 (Figure 5 and Table 1). This subduction zone  
442 clearly questions the origin of the high uplift rate: the extensional setting, the proximity to  
443 slab edges, the subduction of asperities like the d'Entrecasteaux ridge (Collot et al. 1985;  
444 Taylor et al. 2005), or a slab break-off (Châtelain et al. 1992)? A distribution of decreasing

445 uplift rates westward from the trench to the back arc basins is also clearly documented here  
446 (e.g., Collot et al. 1985; Châtelain et al. 1992; Taylor et al., 1987; 2005).

447 (2) The Nazca plate subduction under South America is characterized by a C3 tectonic setting  
448 and a moderate uplift rate (median at 0.176 mm/y and range 0.024-0.816 mm/yr; see also the  
449 transect Figure 3); none of the points is at (or near) a slab edge. A particular characteristic of  
450 this subduction zone is the entrance of some aseismic ridges into the subduction zone  
451 (Gutscher et al., 2000), causing the highest uplift values of this area (e.g., Machare and  
452 Ortlieb (1992); Martinod et al. (2013); Regard et al. (2010); Saillard et al. (2011)). Of  
453 particular interest is the Nazca Ridge entering into the subduction zone in central-south Peru  
454 (Machare and Ortlieb (1992); Regard et al. (2010); Saillard et al. (2011)). The contact point of  
455 the ridge with the trench is moving southeastward (Hampel (2002), Espurt et al. (2008)).  
456 North of this contact point the coastline is subsiding (cf. in Lima, Leroux et al. (2000)), after  
457 the Nazca Ridge passed through. Thus the slab buoyancy appears to be a major driving  
458 parameter for vertical motion in Peru. Another important fact is that if this subduction zone is  
459 characterized by Heuret (2005) as strongly compressive (C3), we note that the forearc  
460 behaves differently: the margin is believed to be tectonically erosional (e.g., Lallemand et al.  
461 (1992)) and it is sometimes extensional, in particular in the entire northern part of Chile (e.g.,  
462 Gonzalez et al., 2003).

463  
464 Finally, these examples show that the uplift rate recorded by ancient shorelines mostly  
465 concerns the forearc, whose tectonic setting (~100-300 km from the trench) is sometimes  
466 disconnected from that of the back-arc area as recorded by Heuret and Lallemand (2005)  
467 (~300-500 km). We can hypothesize that the upper plate quickly responds vertically to  
468 external factors, as every change in geodynamical setting. Consequently, the subduction zones  
469 are generally close to equilibrium with the external forces causing stability (or slowly  
470 evolving) in terms of vertical motion. Superimposed on to this geodynamic setting a ridge  
471 entrance into subduction is prone to cause significant uplift, maybe more efficiently if the far  
472 field upper plate tectonic setting is extensional. That is why high uplift rates are transient and  
473 cannot last more than a couple of hundred of thousand years: figure 10 shows that high uplift  
474 rates are only found in places uplifting for a short period of time (<1-2 My). The ridge effect  
475 is important when the ridge slides along the trench as the Nazca Ridge does (or when a new  
476 ridge enters into trench). On the contrary a ridge entering the subduction at the same point for  
477 a long time would not cause a temporal change: a good example is the Juan Fernandez Ridge  
478 in Chile.



479 *Figure 10. Uplift rate since MIS5 as a function of the observed duration of uplift (maximum age of*  
 480 *uplifted shorelines).*  
 481

## 482 5. CONCLUSION

483 We explored the relationship between the observed coastal late Pleistocene uplift rates and  
 484 various geodynamic parameters. This statistical study shows that most of the geodynamic  
 485 parameters are not related to coastal uplift magnitude. The distance to the trench presents a  
 486 slightly correlated signal with the coastal uplift. It is possible this effect ends at ~300 km from  
 487 the trench, which approximately corresponds to the position of the volcanic arc. Other slight  
 488 correlations have been found between uplift and slab dip, position along the trench and  
 489 overriding plate tectonic regime.

490 The main message is that subduction zones are characterized by rapid vertical motion (uplift  
 491 but maybe also subsidence as stated in introduction), only part of which being satisfactorily  
 492 explained by the geodynamic setting. Over this global setting, strong vertical motion is due to  
 493 smaller scale heterogeneities (one can call roughness) of the subducting plate, one typical  
 494 example of roughness being a subducting aseismic ridge. Asperity affects more efficiently the  
 495 areas close to the trench.

## 496 ACKNOWLEDGEMENTS

497 This study is based on a dataset produced in the framework of the ANR JCJC GISELE  
 498 (Geodynamics of Sea Level, PI. L. Husson) with a support from the INSU/SHOM reliefs de la  
 499 Terre program “erosion of rocky coasts” (PI V. Regard). We thank W. P. Schellart (Associated  
 500 Editor), M.-A. Gutscher and an anonymous reviewer for their constructive comments.

## 501 REFERENCES

502  
 503 Becker, T.W., 2006. On the effect of temperature and strain-rate dependent viscosity on global  
 504 mantle flow, net rotation, and plate-driving forces. *Geophys. J. Int.* 167, 943–957.  
 505 doi:10.1111/j.1365-246X.2006.03172.x

506 Becker, T.W., 2008. Azimuthal seismic anisotropy constrains net rotation of the lithosphere.  
507 Geophys. Res. Lett. 35, L05303. doi:10.1029/2007GL032928

508 Châtelain, J.-L., Molnar, P., Prévot, R., and Isacks, B.L., 1992. Detachment of part of the  
509 downgoing slab and uplift of the New Hebrides (Vanuatu) islands. Geophysical  
510 Research Letters 19, 1507–1510.

511 Clift, P., Vannucchi, P., 2004. Controls on tectonic accretion versus erosion in subduction  
512 zones: Implications for the origin and recycling of the continental crust. Reviews of  
513 Geophysics 42, 2003RG000127.

514 Conrad, C. and Husson, L., 2009. Influence of dynamic topography on sea level and its rate of  
515 change. Lithosphere, 1(2): 110-120, doi: 10.1130/L32.1.

516 Collot, J. Y., Daniel J., and Burne R.V., 1985. Recent tectonics associated with the  
517 subduction/collision of the d'Entrecasteaux Zone in the central New Hebrides:  
518 Structures and processes in subduction zones, Tectonophysics, 112, 325 – 356.

519 DeMets, C., Gordon, R.G., Argus, D.F. and Stein, S., 1994. Effect of recent revisions to the  
520 geomagnetic reversal time scale on estimates of current plate motions. Geophysical  
521 Research Letters, 21(20): 2191-2194.

522 Espurt, N., Funiciello, F., Martinod, J., Guillaume, B., Regard, V., Faccenna, C. and Brusset,  
523 S., 2008. Flat subduction dynamics and deformation of the South American plate:  
524 Insights from analog modeling. Tectonics, 27: TC3011, doi:10.1029/2007TC002175.

525 Funiciello, F., Faccenna, C. and Giardini, D., 2004. Role of lateral mantle flow in the  
526 evolution of subduction systems: insights from laboratory experiments. Geophysical  
527 Journal International, 157: 1393-1406.

528 Funiciello, F., Moroni, M., Piromallo, C., Faccenna, C., Cenedese, A. and Bui, H.A., 2006.  
529 Mapping mantle flow during retreating subduction: Laboratory models analyzed by  
530 feature tracking. Journal of Geophysical Research - Solid Earth, 111: B03402,  
531 doi:10.1029/2005JB003792.

532 Funiciello, F., Faccenna, C., Heuret, A., Lallemand, S., Di Giuseppe, E., Becker, T.W., 2008.  
533 Trench migration, net rotation and slab–mantle coupling. Earth and Planetary Science  
534 Letters 271: 233–240.

535 Gonzalez, G., Cembrano, J., Carrizo, D., Macci, A. and Schneider, H., 2003. The link between  
536 forearc tectonics and Pliocene-Quaternary deformation of the Coastal Cordillera,  
537 northern Chile. Journal of South American Earth Sciences, 16: 321-342.

538 Gripp, A.E., Gordon, R.G., 2002. Young tracks of hotspots and current plate velocities.  
539 Geophysical Journal International 150, 321–361.

540 Guillaume, B., Moroni, M., Funiciello, F., Martinod, J. and Faccenna, C., 2010. Mantle flow  
541 and dynamic topography associated with slab window opening: Insights from  
542 laboratory models. Tectonophysics, 496: 83-98.

543 Gutscher, M.A., Malavieille, A., Lallemand, S. and Collot, J.Y., 1999a. Tectonic segmentation  
544 of the North Andean margin: impact of the Carnegie Ridge collision. Earth and  
545 Planetary Science Letters, 168: 255-270.

546 Gutscher, M.A., Olivet, J.L., Aslanian, D., Eissen, J.P. and Maury, R., 1999b. The “Lost Inca  
547 Plateau”: cause of flat subduction beneath Peru? Earth and Planetary Science Letters,  
548 171: 335-341.

549 Gutscher, M.A., Spakman, W., Bijwaard, H. and Engdhal, E.R., 2000. Geodynamics of flat  
550 subduction: Seismicity and tomographic constraints from the Andean margin.  
551 Tectonics, 19(5): 814-833.

552 Hampel, A., 2002. The migration history of the Nazca Ridge along the Peruvian active  
553 margin: a re-evaluation. Earth and Planetary Science Letters, 203(665-679).

554 Heuret, A., 2005. Dynamique des zones de subduction: étude statistique globale et approche  
555 analogique, PhD, University of Montpellier, 241 p.

556 Heuret, A., Lallemand, S., 2005. Plate motions, slab dynamics and back-arc deformation.  
557 Physics of the Earth and Planetary Interiors 149: 31–51.

558 Husson, L., 2012. Trench migration and upper plate strain over a convecting mantle. Physics  
559 of the Earth and Planetary Interiors, 212-213: 32-43.

560 Kopp, R.E., Simons, F.J., Mitrovica, J.X., Maloof, A.C. and Oppenheimer, M., 2009.  
561 Probabilistic assessment of sea level during the last interglacial stage. Nature, 462:  
562 863-867.

563 Kreemer, C., 2009. Absolute plate motions constrained by shear wave splitting orientations  
564 with implications for hot spot motions and mantle flow. J. Geophys. Res.-Solid Earth  
565 114, B10405. doi:10.1029/2009JB006416

566 Lajoie, K.R., Ponti, D.J., II, C.L.P., Mathieson, S.A. and Sarna-Wojcicki, A.M., 1991.  
567 Emergent marine strandlines and associated sediments, coastal California; a record of  
568 Quaternary sea-level fluctuations, vertical tectonic movements, climatic changes, and  
569 coastal processes, in: Quaternary Nonglacial Geology: Conterminous U.S. Geological  
570 Society of America, Boulder, Colorado: 190-203.

571 Lallemand, S., 1999. La subduction océanique. Gordon and Breach Science Publishers.

572 Lallemand, S., Heuret, A. and Boutelier, D., 2005. On the relationships between slab dip,  
573 back-arc stress, upper plate absolute motion, and crustal nature in subduction zones.  
574 Geochemistry, Geophysics, Geosystems, 6: Q09006, doi:10.1029/2005GC000917.

575 Lallemand, S., Schnurle, P. and Manoussis, S., 1992. Reconstruction of Subduction Zone  
576 Paleogeometries and Quantification of Upper Plate Material Losses Caused by  
577 Tectonic Erosion. Journal of Geophysical Research, 97: 217-239.

578 Leroux, J.P., Correa, C.T. and Alayza, F., 2000. Sedimentology of the Rimac-Chillon alluvial  
579 fan at Lime, Peru, as related to Plio-Pleistocene sea-level changes, glacial cycles and  
580 tectonics. Journal Of South American Earth Sciences, 13: 499-510.

581 Lowry, A.R., Ribe, N.M. and Smith, R.B., 2000. Dynamic elevation of the Cordillera, western  
582 United States. Journal of Geophysical Research: Solid Earth, 105: 23371-23390.

583 Machare, J. and Ortlieb, L., 1992. Plio-Quaternary vertical motions and the subduction of the  
584 Nazca Ridge, central coast of Peru. Tectonophysics, 205: 97-108.

585 Martinod, J., Guillaume, B., Espurt, N., Faccenna, C., Funicello, F. and Regard, V., 2013.  
586 Effect of aseismic ridge subduction on slab geometry and overriding plate  
587 deformation: Insights from analogue modeling. Tectonophysics, 588: 39-55.

588 Müller, R., Roest, W., Royer, J.Y., Gahagan, L. and Sclater, J., 1997. Digital isochrons of the  
589 world's ocean floor. Journal of Geophysical Research, 104: 3211-3214.

590 Müller, R.D., Sdrolias, M., Gaina, C., Steinberger, B. and Heine, C., 2008. Long-term sea  
591 level fluctuations driven by ocean basin volume change. Science, 319: 1357-1362.

592 O'Leary, M.J., Hearty, P.J., Thompson, W.G., Raymo, M.E., Mitrovica, J.X. and Webster,  
593 J.M., 2013. Ice sheet collapse following a prolonged period of stable sea level during  
594 the last interglacial. Nature Geoscience, 6: 796-800.

595 O'Neill, C., Müller, D., Steinberger, B., 2005. On the uncertainties in hot spot reconstructions  
596 and the significance of moving hot spot reference frames. Geochem. Geophys.  
597 Geosyst. 6, Q04003. doi:10.1029/2004GC000784

598 Pearson, K., 1896. Mathematical Contributions to the Theory of Evolution. III. Regression,  
599 Heredity and Panmixia. Philosophical Transactions of the Royal Society of London  
600 187: 253-318.

601 Pedoja, K., Husson, L., Johnson, M.E., Melnick, D., Witt, C., Pochat, S., Mexer, M.,  
602 Delcaillau, B., Pinegina, T., Poprawski, Y., Authemayou, C., Elliot, M., Regard, V. and  
603 Garestier, F., in press. Staircase construction of Quaternary and Upper Cenozoic  
604 sequences of strandlines caused by sea level oscillations and tectonic uplift. Earth-  
605 Science Reviews, in press.

606 Pedoja, K., Husson, L., Regard, V., Cobbold, P.R., Ostanciaux, E., Johnson, M.E., Kershaw,  
607 S., Saillard, M., Martinod, J., Gurgerot, L., Weill, P. and Delcaillau, B., 2011. Relative  
608 sea-level fall since the last interglacial stage: Are coast uplifting worldwide? *Earth-*  
609 *Science Review*, 108: 1-15.

610 Pirazzoli, P.A., Radtke, U., Hantoro, W.S., Jouannic, C., Hoang, C.T., Causse, C. and Besth,  
611 M.B., 1993. A one million-year-long sequence of marine terraces on Sumba Island,  
612 Indonesia. *Marine Geology*, 109: 221-236.

613 RDevelopment Core Team, 2010. R: A language and environment for statistical computing. R  
614 Foundation for Statistical Computing <http://www.R-project.org/>.

615 Regard, V., Saillard, M., Martinod, J., Audin, L., Carretier, S., Pedoja, K., Riquelme, R.,  
616 Paredes, P. and Hérail, G., 2010. Renewed uplift of the Central Andes Forearc revealed  
617 by coastal evolution during the Quaternary. *Earth and Planetary Science Letters*, 297:  
618 199-210.

619 Saillard, M., Hall, S.R., Audin, L., Farber, D.L., Regard, V. and Hérail, G., 2011. Andean  
620 coastal uplift and active tectonics in southern Peru: <sup>10</sup>Be surface exposure dating of  
621 differentially uplifted marine terrace sequences (San Juan de Marcona, ~ 15.4°S).  
622 *Geomorphology*, 128: 178-190.

623 Schellart, W.P., 2011. A subduction zone reference frame based on slab geometry and  
624 subduction partitioning of plate motion and trench migration. *Geophys. Res. Lett.* 38,  
625 L16317. doi:10.1029/2011GL048197

626 Schellart, W.P., Freeman, J., Stegman, D.R., Moresi, L. and May, D., 2007. Evolution and  
627 diversity of subduction zones controlled by slab width. *Nature*, 446: 308-311.

628 Schellart, W.P., Stegman, D.R., Farrington, R.J. and Moresi, L., 2011. Influence of lateral slab  
629 edge distance on plate velocity, trench velocity, and subduction partitioning. *Journal of*  
630 *Geophysical Research - Solid Earth*, 116: B10408, doi:10.1029/2011JB008535.

631 Schellart, W.P., Stegman, D.R., Freeman, J., 2008. Global trench migration velocities and slab  
632 migration induced upper mantle volume fluxes: Constraints to find an Earth reference  
633 frame based on minimizing viscous dissipation. *Earth-Sci. Rev.* 88, 118–144.  
634 doi:10.1016/j.earscirev.2008.01.005

635 Sella, G.F., Dixon, T.H. and Mao, A.L., 2002. REVEL: A model for recent plate velocities  
636 from space geodesy. *Journal of Geophysical Research - Solid Earth*, 107(B4): ETG-11,  
637 doi:10.1029/2000JB000033.

638 Stafford, K., Mylroie, J., Taborosi, D., Jenson, J. and Mylroie, J., 2005. Karst development on  
639 Tinian, commonwealth of the Northern Mariana Islands: Controls on dissolution in  
640 relation to the Carbonate Island Karst Model. *Journal of Cave and Karst studies*, 67:  
641 14-27.

642 Steinberger, B., Sutherland, R. and O'Connell, R.J., 2004. Prediction of Emperor-Hawaii  
643 seamount locations from a revised model of global plate motion and mantle flow.  
644 *Nature*, 430: 167-173.

645 Tassara, A., 2005. Interaction between the Nazca and South American plates and formation of  
646 the Altiplano–Puna plateau: Review of a flexural analysis along the Andean margin  
647 (15°–34°S). *Tectonophysics*, 399: 39-57.

648 Tassara, A., Hackney, C. and Kirby, R., 2007. Elastic thickness structure of South America  
649 estimated using wavelets and satellite-derived gravity data. *Earth and Planetary*  
650 *Science Letters*, 253: 17-36.

651 Taylor, F.W., Frohlich, C., Lecolle, J., Strecker, M., 1987. Analysis of partially emerged  
652 corals and reef terraces in the central Vanuatu Arc: Comparison of contemporary  
653 coseismic and nonseismic with quaternary vertical movements. *Journal of*  
654 *Geophysical Research: Solid Earth* 92, 4905–4933.

655 Taylor, F.W., Mann, P., Bevis, M.G., Edwards, R.L., Cheng, H., Cutler, K.B., Gray, S.C., Burr,  
656 G.S., Beck, J.W., Phillips, D.A., Cabioch, G. and Recy, J., 2005. Rapid forearc uplift  
657 and subsidence caused by impinging bathymetric features: Examples from the New  
658 Hebrides and Solomon arcs. *Tectonics*, 24: TC6005, doi:10.1029/2004TC001650.

659 Tukey, J.W., 1977. *Exploratory data analysis*, Addison-Wesley Series in Behavioral Science:  
660 Quantitative Methods, Reading, Mass., vol. 1 Addison-Wesley.

661 Waelbroeck, C., Labeyrie, L., Michel, E., Duplessy, J.C., McManus, J.F., Lambeck, K. and  
662 Labracherie, M., 2002. Sea level and deep water temperature changes derived from  
663 benthics foraminifera isotopic records. *Quaternary science reviews*, 21(1-3): 295-305.

664 Yañez, G.A., Ranero, C.R., Huene, R.v. and Diaz, J., 2001. Magnetic anomaly interpretation  
665 across the southern central Andes (32 degrees-34 degrees S): The role of the Juan  
666 Fernandez Ridge in the late Tertiary evolution of the margin. *Journal of Geophysical*  
667 *Research-Solid Earth*, 106: 6325-6345.

668  
669